Solar photocatalysis of TiO2 supported natural palygorskite nanofibers elaborated by a one_pot mechanochemical route

Omar Lakbita, Benaissa Rhouta, Vincent Goetz, Francis Maury, Gael Plantard, Lahcen Daoudi

Solar photocatalysis of TiO_2 supported natural palygorskite nanofibers elaborated by a one_pot mechanochemical route

Lakbita Omar[1], Rhouta Benaissa[2*], Goetz Vincent[3], Maury Francis[4], Plantard Gaël[3], Daoudi Lahcen[5]

[1] Chemical & Biochemical Sciences (CBS), Green Process Engineering, Mohammed VI Polytechnic University (UM6P). Lot 660, Hay Moulay Rachid, 43150 Ben Guerir, Maroc.

[2] IMED_Lab, Faculty of Sciences and Technologies, Cadi Ayyad University, Box 549, 40000 Marrakech, Morocco.

[3] PROcédés Matériaux et Energie Solaire, Rambla de la Thermodynamique, PROMES_CNRS, UPR 8521, 66100 Perpignan cedex, France.

[4] CIRIMAT, Université de Toulouse, CNRS_UPS_INP, 4 allée Emile Monso, BP 44362, 31030 Toulouse, cedex 4, France.

[5] Laboratoire de Geoscience et Géoenvironnement, Faculté des Sciences et Techniques Guéliz, Université Cadi Ayyad, BP 549, Marrakech, Maroc.

* E-mail address of the corresponding author: plantard@univ-perp.fr

Abstract:

This study reports the successful synthesis of supported TiO_2_Palygorskite nanocomposites by a one-pot dry mechanochemical route. Indeed, the elaboration procedure involved an in-situ reaction between accessories carbonates present in raw fibrous palygorskite clay and titanyl sulfate ($TiOSO_4$) precursor under variable grinding conditions, essentially ball/solid matter mass ratio and rotation velocity. This yielded after air annealing at 600°C for 1 h to the immobilization of anatase TiO_2 nanoparticles (≈ 8 nm of average size) as evidenced by XRD and TEM analyses. Once the conditions of elaboration were optimised, the photocatalytic properties were evaluated under 3 conditions: artificial UV radiation, artificial solar radiation (UV+visible range) and under dynamic solar illumination taking into account the discontinuities of the solar resource. The results allowed the estimation and comparison of the catalyst's capabilities and showed its ability to work under natural irradiation. The so developed supported photocatalysts TiO_2/Palygorskite exhibited a good activity towards the removal of Orange G (OG) dye from aqueous media under artificial UV and natural solar radiations.

Keywords: TiO_2, palygorskite, mechanochemical synthesis, nanocomposite, solar photocatalysis, wastewater treatment.

1. Introduction

Heterogeneous photocatalytic oxidation recently has emerged as an efficient alternative process for wastewater treatment [1–6]. The principle of this technique relies on the creation of reactive species as holes (h^+) and hydroxyl radicals ($OH^\bullet$) upon irradiating a semiconductor oxide with an energy source ($h\upsilon$) higher than its energy band gap [1,6]. In optimized processes, the highly oxidizing species so generated are able to induce complete mineralization of organic pollutants into CO_2 and H_2O **[1]**. TiO_2 anatase is the most active semiconductor oxide in photocatalysis and is besides widely used owing to its numerous advantages, for instance, non-harmfulness, low cost, and chemical inertness [1]. Several wet methods, including sol-gel [7–9], flame aerosol [10], solvothermal [11] were reported for the synthesis of TiO_2 powder. Interestingly, a dry method based on grinding powders of carbonate compound, namely Na_2CO_3 and a Ti molecular precursor such as titanium sulfide (TiS_2) [12,13] and titanyl sulfate ($(TiOSO_4{\cdot}2H_2O)$ [14–16] was also reported to synthesize pure TiO_2 powder. However, the direct use of TiO_2 in the form of nano-powder (*e.g.*, commercial Degussa P25 powder [10]) raises several problems such as agglomeration of the nanoparticles during the process, which reduces photocatalytic efficiency [17]. Additionally, recovering of micron sized aggregated particles from water decontaminated by TiO_2 slurry needs to implement costly microfiltration processes [2,6,17,18]. To overcome these drawbacks, researches focused on improving photocatalytic processes by the development of TiO_2 supported photocatalysts, in particular starting with natural highly dispersed materials as support.

The solar resource is a sustainable energy by definition and available for many applications. For photo-oxidation applications, capacities are limited because most catalysts are only sensitive to ultra violet (UV) radiation in the spectrum. This represents only 5% of the solar radiation, resulting in limited performance for solar installations. A second characteristic of the solar resource is its intermittent nature, which is due to the daily (day/night) and seasonal cycle,

but also to meteorological effects such as the passage of clouds or heavy cloud cover. Thus, to meet these constraints, the catalysts developed must have photocatalytic properties that allow the use of the solar resource and manage the fluctuations linked to this resource. This implies catalysts with both photo-excitation characteristics to produce radicals and sorption characteristics to store the molecules during low sunlight phases.

Among the support materials envisaged, clay minerals are considered promising owing to their interesting inherent multi-functional properties such as their adsorption capacity, high surface area, multiscale porosity, and ability to be grafted by chemical compounds [18–25]. In this respect, some authors more recently reported CeO_2_WO_3_Palygorskite/TiO_2 catalysts elaborated by impregnation method [26] and TiO_2 supported on three natural clays with different morphologies carried out by sol-gel route [27]. In the same way, we reported some years ago the immobilization of TiO_2 anatase nanoparticles (NPs) with an average size of 10 nm onto particles surfaces of beidellite [28] and nanofibers surfaces of palygorskite [29] via a colloidal sol-gel route. Beidellite and palygorskite were both natural clay minerals sampled in Morocco from Agadir basin and Marrakech High Atlas regions, respectively. They were purified, characterized, and specifically functionalized to be used as catalytic supports in the wet synthesis methods employed [30,31]. Photocatalytic tests performed in presence of these TiO_2 supported clay nanocomposites towards the degradation of Orange G dye (OG) were promising in that they interestingly exhibited a photoactivity normalized to the TiO_2 amount higher than that of pure TiO_2 micropowder commercially available as Degussa P25.

Nevertheless, the synthesis of these supported photocatalysts is generally achieved via colloidal [21,29] or solvothermal [32] or pillaring [20] wet routes, which on one hand required previous purifying and/or homoionisation with Na^+ ions of clay minerals. On the other hand, these elaboration methods involved several steps so that they are laborious, time and solvents consuming and yielding to small laboratory amounts. Thereby, they have a low capacity to be

transferred to industrial scale. Thus, there is a need to find out alternative synthesis method to overcome these wet routes issues.

The aim of this work is to show the potential of these materials for a solar photo-oxidation application. It is divided into three parts. The first part aims at elaborating TiO_2 supported palygorskite by a free-solvent one-pot mechanochemical method starting from powders of raw palygorskite (Pal) clay and titanyl sulfate ($TiOSO_4 \cdot 2H_2O$) precursor. This dry synthesis route was smartly based on *in-situ* reaction between carbonates accessorily available in raw clay and a Ti molecular precursor to immobilize resulting TiO_2 particles on the surface of palygorskite fibers or in the vicinity of their surface in the tangle of fibers. Synthesis conditions were optimized by studying the influence of the composition ratio palygorskite clay / $TiOSO_4 \cdot 2H_2O$ and grinding velocity. The second step is to select the optimal conditions for the development of a material in order to control the photocatalytic properties. The so elaborated TiO_2–Pal nanocomposites were afterwards characterized at a multi-scale level using *in situ* X-ray diffraction (XRD (X'pert powders Philips diffractometer)), Scanning Electron Microscopy (SEM (SEM-FEG, Hitachi S-4500)) and Transmission Electron Microscopy (TEM (JEOL JEM 2010)). The originality lies in a global approach starting from the elaboration of the catalysts, their optimization to test their photocatalytic potential. The aim being to evaluate the photo-oxidation capacities under solar conditions, our step-by-step approach involves three stages. Measurements are carried out under controlled irradiation conditions, both in terms of spectral distribution and flux density (artificial UV and solar irradiation) with the aim of modelling the photo-oxidative capacities of the catalysts. Finally, the photo-oxidation capacities are measured and modelled under natural irradiation, taking into account the characteristics of solar radiation: spectral distribution and flux density discontinuities. Thus, photo-activities were evaluated towards the removal from aqueous medium of Orange dye (OG) considered as a model pollutant

under UV radiations and solar light by using indoor lab-scale reactors equipped with an artificial solar light and a larger outdoor pilot irradiated by natural solar light.

2. Experimental details

2.1- Materials and synthesis

Natural raw clay, involved herein, was sampled from Marrakesh – High Atlas region. Detailed characterizations performed by Rhouta *et al*. [30] on this clay revealed that it is made up of fine clay fraction (< 2 μm) (> 65%) along with accessory minerals, namely quartz (< 5%) and carbonates (≈ 30 wt%) in the forms of calcite ($Mg_{0.03}Ca_{0.97}CO_3$) and ankerite ($Ca_{1.01}Mg_{0.45}Fe_{0.54}(CO_3)_2$). The extracted fine fraction (< 2 μm) was found to be exclusively composed of fibrous clay minerals, namely palygorskite (≈ 95%) exhibiting predominant dioctahedral character and deficiency into zeolitic water along with sepiolite (≈ 5%). The composition of this palygorskite was found on the basis of 26 oxygens to be $(Si_{7.97}Al_{0.03})(Mg_{2.17}Al_{1.46}Fe_{0.40}Ti_{0.05})(Ca_{0.03}Na_{0.07}K_{0,03})O_{20.18}(OH)_{1.94}(H_2O)_{3.88}$, 2.43 H_2O. Its Cation Exchange Capacity (CEC), Brunaeur-Emmet-Teller method (BET) specific surface area and total porous volume were assessed to be 21.2 meq.100 g^{-1}, 116 $m^2.g^{-1}$ and 0.458 $cm^3.g^{-1}$ respectively.

The Ti precursor considered herein is the titanyl sulfate ($TiOSO_4{\cdot}2H_2O$) purchased from Aldrich and used without further treatment.

In contrast to our previous works [24-27, 30] in which the synthesis of clay minerals supported photocatalysts implied several laborious and time-consuming steps including purifying, homoionisation and fine fraction recovering before its functionalization, the elaboration herein was accomplished according to a one-pot route starting directly from raw clay. Indeed, given amounts of raw palygorskite clay and $TiOSO_4{\cdot}2H_2O$ powders were introduced in an alumina jar of planetary ball mill PM100 from Retsch for being grinded using six alumina balls of 20 mm in diameter. The synthesis of TiO_2 supported on palygorskite fibers was achieved by *in-*

situ reacting carbonates accessorily present (≈ 30 wt%) in raw clay with $TiOSO_4 \cdot 2H_2O$ precursor according to different conditions. Indeed, the amount of each reactant was chosen in such a way to have a total mass of reactants of 50 g per run by considering two raw clay / $TiOSO_4$ mass ratios of 0.6/1 and 3.3 /1, which corresponded to mixtures in which both compounds were in stoichiometric or in excess proportions, respectively. The grinding was performed at a rate of 500 rpm for different times (10, 15, 20 and 30 min). As-grinded samples were thereafter air annealed for 1 h at different temperatures (400, 500, 600 and 700°C). Samples were designated Pal_TiO_2(x)_G_y_T_z by referring to the composite nature of the sample (Pal_TiO_2), the reactant mass ratio (x= TiO_2/Pal), the grinding time (G_y) and the post-heat-treatment temperature (T_z). The obtained powdered materials were finally stored for further uses.

2.2- Characterizations

The structural changes of TiO_2 upon heating of as-grinded samples were analyzed *in situ* versus the temperature by XRD over the two-theta range 2_60 deg using a Bruker D8 Advance diffractometer equipped with a Vantec Super Speed detector and an Mid- Infrared (MIR) radiation heating chamber (Bragg-Brentano configuration; Ni filtered Cu K_α radiation). The diffractograms were recorded every 50°C from the room temperature to 950°C. An isotherm was maintained at each level for 40 min to record the pattern then the temperature was increased using a ramp of 1 deg.s^{-1} up to the next level. Also XRD at room temperature was recorded on TiO_2_Pal samples prior to air annealing at different temperatures in the same angular range using a Seifert XRD 3000TT diffractometer equipped with a graphite monochromator (Bragg-Brentano configuration; Cu K_α radiation).

The microstructure, morphology and uniformity of the samples were analyzed at different steps of the synthesis by a Scanning Electron Microscope (SEM; Leo-435VP)

equipped with an Oxford energy dispersive spectrometer (EDS, (EDS, KEVEX Si(Li) assisted software Brüker)). Also, a JEOL JEM 2010 TEM equipped with a Tracor EDS analyzer was used for characterizing clay particles and performing local elemental composition.

2.3- Photocatalytic activity

The photocatalytic activity of different samples was evaluated using three kinds of set-ups: a laboratory-scale set-up, an indoor solar simulator and an outdoor solar pilot.

As far as the first set-up is concerned, the degradation reaction was performed in a batch quartz reactor ($40 \times 20 \times 36$ mm^3) placed in a thermostated chamber (25°C) under the UV light of a lamp (HPLN Philips 125 W) emitting at 365 nm. The reactor was irradiated with a photon flux of about 100 $mW.cm^{-2}$ by adjusting the distance to the lamp so that it simulates the UV intensity of solar spectrum on the earth [33]. This lamp was chosen because the OG absorption is negligible at this wavelength and, as a result, the direct photolysis of the solution (*i.e.* without photocatalyst) was found negligible for more than 24 h. The photoactivity of different samples was assessed at pH around 6 by measuring the decomposition rate of OG in aqueous solutions containing the supported photocatalyst according to a procedure previously reported [34] and adapted to the dispersion of supported powder photocatalysts in previous papers [28,35]. The photocatalyst powder of TiO_2_Pal nanocomposites was added to 25 cm^3 of OG solution (10^{-5} M) in an amount equal to 0.8 $g.dm^{-3}$. This catalyst mass was found as optimum to avoid excess of catalyst and to ensure an efficient absorption of photons [36]. The dispersion was agitated with an inert Teflon magnetic stirrer. To determine the dye concentration, aliquots were taken from the mixture at regular time intervals and centrifuged at 12500 rpm for 5 min. The OG concentration in the supernatant was determined by measuring the absorbance at 480 nm using a UV-VIS-NIR spectrophotometer (Perking Elmer lambda 19).

Sunlight is particularly weak in the UV spectral region and, in addition, it changes along the day due to day-night and seasonal cycles [37,38]. Thus, prior optical and kinetic studies have to be performed to determine on one hand optimal catalyst mass allowing the maximum (≈ 90%) of the absorption of photons (considered as reactant) and, on the other hand, kinetic constants to achieve process efficiency in an outdoor solar pilot [37,39]. Therefore, optical properties of photocatalysts suspensions differing in mass concentrations were studied by an optical experimental setup described in details elsewhere [37,39]. Practically, the light supplied by a source simulating solar radiation (maximum intensity equal to 1000 $W.m^{-2}$ in the full spectral range, *i.e.* 50 $W_{uv}.m^{-2}$ in the UV range) came across a Polymethyl methacrylate (PMMA treated to be UVA transparent, Sunactive® GS2458) cell 2 cm thick (*i.e.* optical length) containing under stirring the TiO_2_Pal dispersions whose concentrations ranged from 0.1 to 4 $g.L^{-1}$. This cell was placed at the inlet of an integrating sphere. The direct radiation as well as scattered radiation transmitted hence collected from the integration sphere were directed via an optical fiber towards a spectrophotometer permitting the detection of wavelengths ranging from 250 to 1100 nm (ultraviolet, visible and near-infrared). The transmission of light was hence assessed versus catalyst powder concentration to determine the mass concentration at which the 90% absorbency was reached. Afterwards, kinetic study of OG dye degradation was carried out versus mass concentration of catalysts powders dispersion by using an indoor solar simulator set-up. For a given mass concentration the catalyst dispersion was kept under stirring in a 150 mL quartz bucker (suspension height of 5 cm), then it was irradiated by sunlight simulator (1000 $W.m^{-2}$) under constant photons flow. At different time intervals, aliquots were picked up from media, centrifuged and resulting supernatants analyzed by spectrophotometry to determine the dye concentration according to the way described above.

Afterwards, the efficiency of TiO_2_Pal catalysts towards the photodegradation under sunlight of OG dye was tested by using an outdoor solar pilot described in details by Janin *et al.*, [40]

(picture given in the supplementary figure 1S). Briefly, a mass concentration of TiO_2_Pal that permitting 90% of photons absorption was dispersed under stirring in an OG dye solution and stored in a stainless steel tank (with a maximum volume of 50 L). Then 6 L of effluent were fed into a flat solar panel ($30 \times 100 \times 2$ cm^3) from the bottom to the top via a liquid pump and recirculated into the thank. This panel was covered with a special PMMA plate to prevent evaporation of compounds and to ensure watertight. This flat reactor was oriented southwards and inclined at an angle around 42° in order to maximize the average solar irradiation throughout the year. This was controlled by two equipments: a pyranometer whose wavelength domain varies between 380 to 2800 nm and an UV radiometer (UVA-Sensor CT-UVA 3) measuring the corresponding spectrum in the range of 310 – 400 nm;

3. Results and discussion

3.1- Structural characterizations

Figure 1 shows an overview of the room temperature XRD diagrams of the two starting materials after a grinding for 30 min at 500 rpm: titanyl oxysulfate precursor ($TiOSO_4$) and palygorskite-rich raw clay (Pal). Also, the XRD diagrams of a mixture of $TiOSO_4$ and Pal clay in a mass ratio of 0.6/1 after grinding for 30 min at 500 rpm is reported (Pal_$TiOSO_4$).

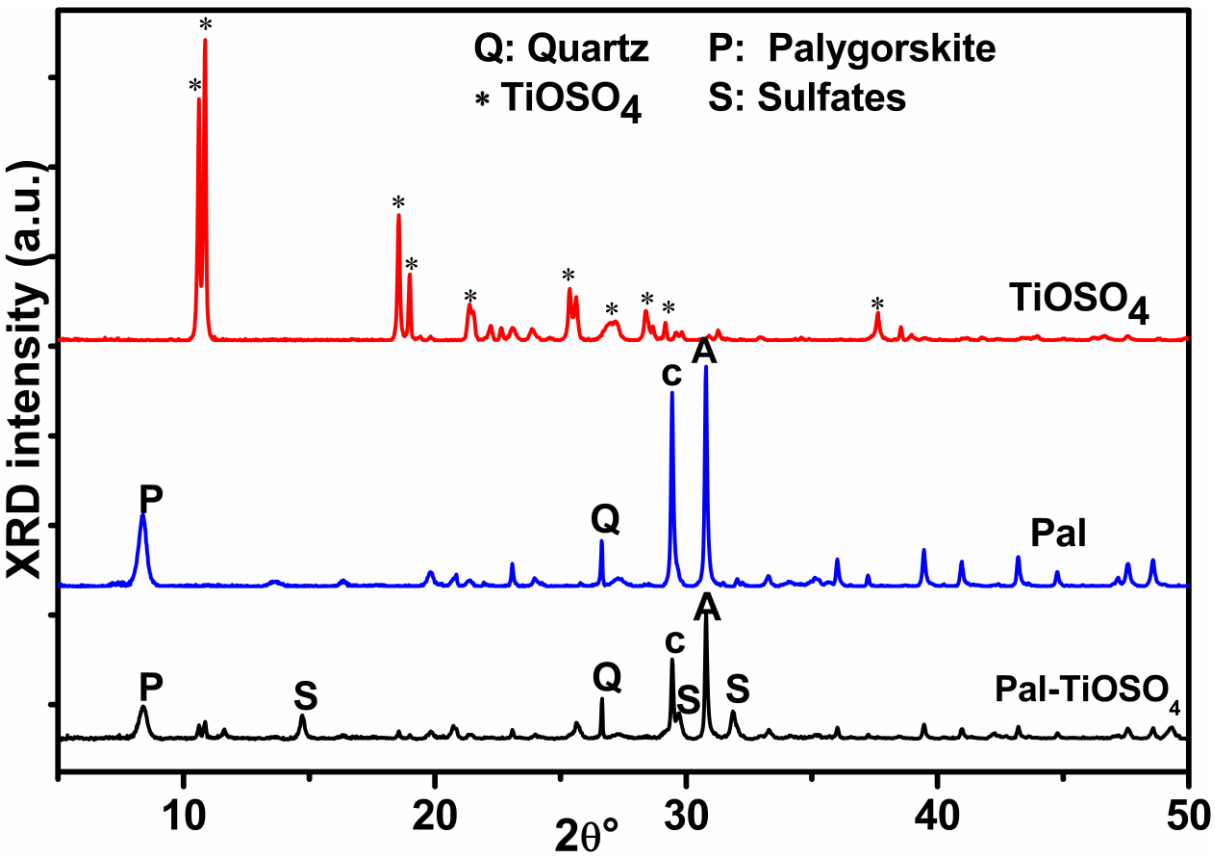

Fig.1: Room temperature XRD patterns of $TiOSO_4$, raw clay (Pal) and Pal_$TiOSO_4$ mixture in mass ratio of 0.6/1 after grinding of each of these samples at 500 rpm for 30 minutes.

The diffractogram pertaining to the milled titanium precursor revealed only the reflections at the 2θ angular positions of 10.67° (8.35 Å), 10.95° (8.20 Å), 18.61° (4.79 Å), 19.07° (4.69 Å), 21.43° (4.16 Å), 25.44° (3.50 Å), 25.70° (3.47 Å), 28.47° (3.13 Å), 29.25° (3.05 Å), 37.70 (2.38 Å), 38.61 (2.33 Å) corresponding to the compound $TiOSO_4$ (ICDD file N°14-503) without evidence for the formation of any other crystalline phase, especially TiO_2. In the same sense, the XRD pattern of the grinded Pal raw clay showed several reflections corresponding to the fibrous mineral, *i.e.* palygorskite, at the angular positions described by Rhouta *et al.*, [30]. The characteristic basal reflection is at 2θ ≈ 8.38° (10.56 Å) in addition to the peaks ascribed to the accessory minerals, namely the carbonates in the form of calcite (C) $Mg_{0.03}Ca_{0.97}CO_3$ (ICDD

file: 01-089-1304) and ankerite (A) $Ca_{1.01}Mg_{0.45}Fe_{0.54}(CO_3)_2$ (ICDD: 01-084-20 2066) as well as quartz (Q) (ICDD file: 03-065-0466) whose strongest reflections were observed at 29.46° (3.03 Å), 30.82° (2.90 Å) and 26.64° (3.34 Å), respectively.

This result showed that both the palygorskite and the accessory phases, constituting the raw Pal clay, were apparently not affected by the grinding operation in the mechanosynthesis jar since their crystallographic structure remained stable. On the other hand, these grinding conditions of the Pal_$TiOSO_4$ mixture caused a drastic decrease in the XRD intensities of $TiOSO_4$ reflexions at the point to disappear, as well as those of the carbonates (calcite and ankerite), while preserving the clay structure confirmed by the persistence of the corresponding peaks. The disappearance of $TiOSO_4$ reflexions can be due to its amorphisation but the major event during grinding is the trigger of reaction (1), according to which $TiOSO_4$ reacts with the carbonates present among the accessory minerals in the raw clay Pal:

$$TiOSO_4{\cdot}2H_2O + Pal/(Na_2,Ca,Mg)CO_3 \rightarrow TiO_2/Pal + (Na_2,Ca,Mg)SO_4,2H_2O + CO_2\uparrow \qquad (1)$$

The occurrence of this reaction was further confirmed by the production of the hydrated sulfate compound $CaSO_4{\cdot}0.5H_2O$ evidenced by the presence in the composite sample Pal_$TiOSO_4$ of the characteristic peaks noted S on the diffractogram (Fig. 1) at angular positions 2θ of 14.71° (6.00 nm), 29.71° (3.00 nm) and 31.86° (2.80 nm) in agreement with the ICDD file 01-081-1848. The near-consumption of the $TiOSO_4$ precursor revealed by XRD may be due to the fact that the low value of the mass ratio $TiOSO_4$:clay (0.6:1) would be the driving force of reaction (1).

Furthermore, the reaction (1) also showed that titanium dioxide has to be formed but no diffraction peaks of this oxide was observed in Figure 1 suggesting that the as-prepared TiO_2 phase must be amorphous after the mechanosynthesis step ($TiOSO_4$:clay = 0.6:1; 500 rpm; 30

min). Subsequently, a mixture of $TiOSO_4$ and Pal raw clay with the mass ratio 3.3/1, *i.e.* with Ti precursor in excess was grinded for 30 min at 500 rpm. Then, XRD patterns of this composite sample were recorded *in-situ* in air as a function of the temperature (Figure 2).

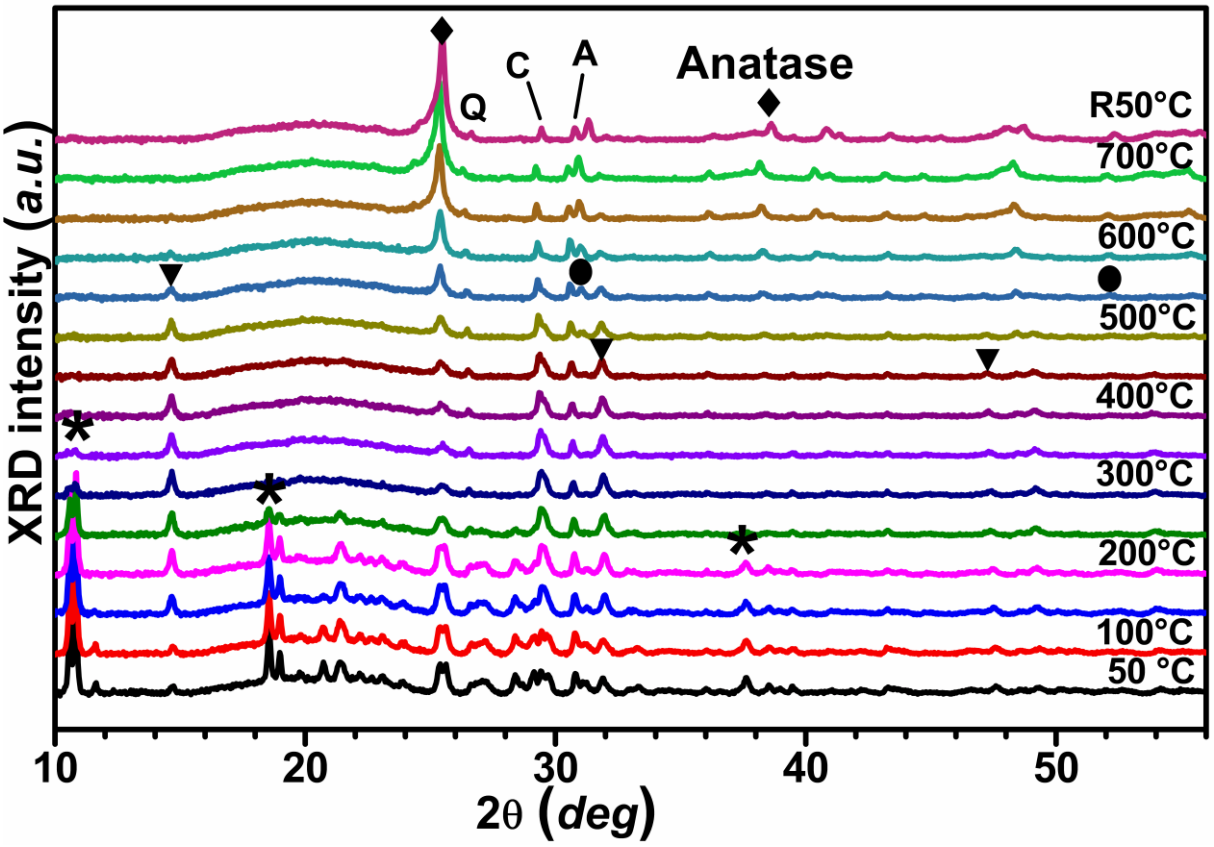

Fig. 2: X-ray diffractograms recorded *in-situ* in air as a function of the sample temperature of a $TiOSO_4$/Pal (3.3/1) mixture after mechanosynthesis (Step 1). These diagrams were recorded every 50°C; they represented the effect of calcination as 2nd step of the synthesis process. They showed the main compounds that disappeared were $TiOSO_4$ (★), calcite (C), ankerite (A), while the compounds that formed were $CaSO_4.xH_2O$ (▼), $CaSO_4$ (●), TiO_2 anatase (♦), and the most thermally stable accessory compounds like quartz (Q).

For as-milled sample, the diagram recorded at 50°C revealed that, as mentioned above, amorphous TiO_2 and the hydrated $CaSO_4$ product were formed during the grinding stage as a

result of the above reaction (1). In this respect, a significant proportion of the carbonates were consumed by the reaction with $TiOSO_4$ (that was in excess) has shown by the decrease of their XRD intensity. This was further supported by a huge decrease in carbonate content determined by coulometric analysis. Indeed, the carbonate content has been reduced approximately by a factor of 2, from 28 ± 2 wt % in the raw clay Pal to 13 ± 2% wt % in the grinded $TiOSO_4$ / Pal (3.3/1) mixture.

By increasing the temperature, it can be seen that the crystallization of anatase TiO_2 started from 450°C as shown by the emergence of the corresponding peaks at angular positions 2θ of about 25.44° (3.51 Å) and 38.53° (2.33Å) (ICDD Data Sheet 01-021-1272). As the temperature increased further, the anatase peaks became more intense and well resolved, indicating the improvement of its crystallization. The anatase peaks remained observable up to 700°C, without the appearance of any XRD peaks of the less photoactive rutile variety. This strongly denoted the remarkable stability of the anatase formed under the conditions of this study. Palygorskite peaks were observable up to 400°C, beyond which their intensities severely reduced. This can be ascribed to the occurrence of structural collapse of the clay mineral. However, this can be also due to an absorption filter induced by the conformal coverage of anatase particles on palygorskite fibers as suggested by Rhouta *et al.*, [28] and Bouna *et al.*, [29] and confirmed by the TEM analyses shown in the next section.

In order to examine the effect of grinding time on the reactivity of $TiOSO_4$ with the carbonates present in the Pal raw clay, a mixture of the two compounds in a ratio of 0.6 / 1 was ground at 500 rpm for 10, 15, 20, 25 and 30 min and then air annealed at 600°C for 1 h. The superimposition of the corresponding XRD diagrams (Fig. 3) clearly showed the formation of anatase TiO_2 for all the samples investigated regardless grinding time. Nevertheless, the anatase crystallinity appeared to improve with the grinding time as evidenced by the gradual narrowing of it characteristic peak at about 2θ around 25°. In this respect, by referring to quartz, which is

an insensible and stable accessory mineral under the applied grinding conditions, the increase of the intensity ratio of the main anatase/quartz peaks is noteworthy. This probably reflected an increase in the amount of anatase phase formed with the increase of grinding time.

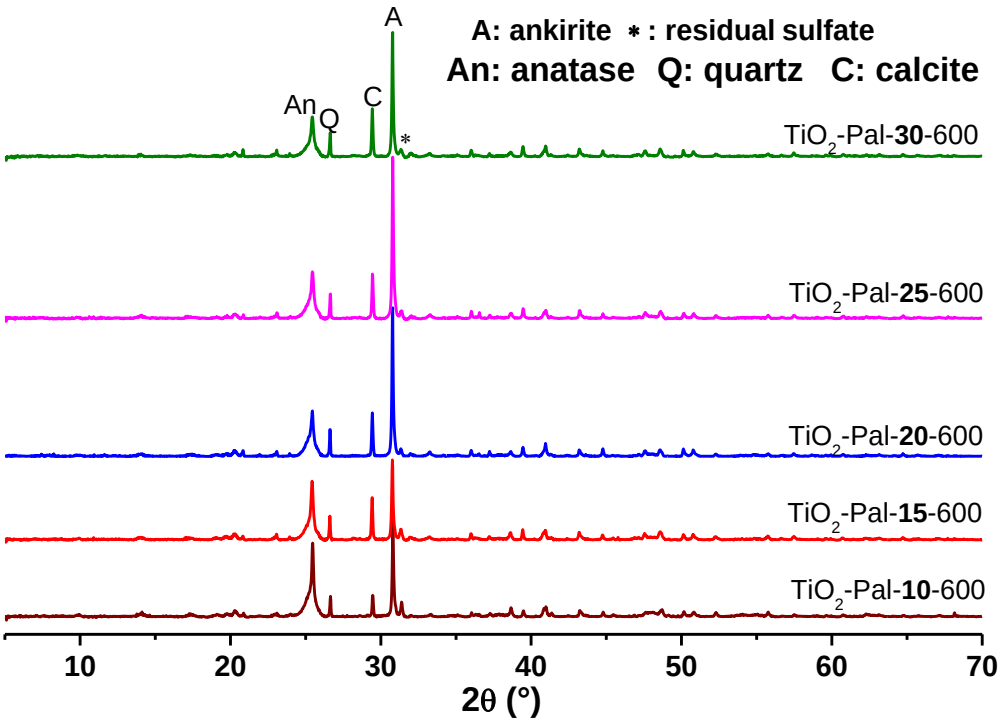

Fig. 3: Stacking of XRD patterns of TiO_2_Pal photocatalysts prepared by grinding $TiOSO_4$ and Pal raw clay in a mass ratio of 0.6/1 during 10, 15, 20, 25 and 30 min at 500 rpm.

3.2- Microstructural characterizations

XRD results were further supported by TEM characterizations. Indeed, depending on the grinding conditions, TEM analysis after the first step showed palygorskite fibers of 30-70 nm in diameter and 650 nm in length mixed with $TiOSO_4$ platelets of 400-600 nm with an average thickness of 3-5 µm. At this stage, no evidence for crystallized anatase nanoparticles (NPs) was found confirming this oxide phase was amorphous. After annealing at 600°C in air for 1 h, TEM revealed that palygorskite fibers were entirely wrapped with homogeneous monodisperse and

spherical TiO_2 anatase NPs 10-15 nm in diameter (Fig. 4a). Only a few palygorskite fibers were not covered as revealed by EDS analysis. For most of them, a granular and conformal TiO_2 coverage formed a uniform cladding (Fig. 4b).

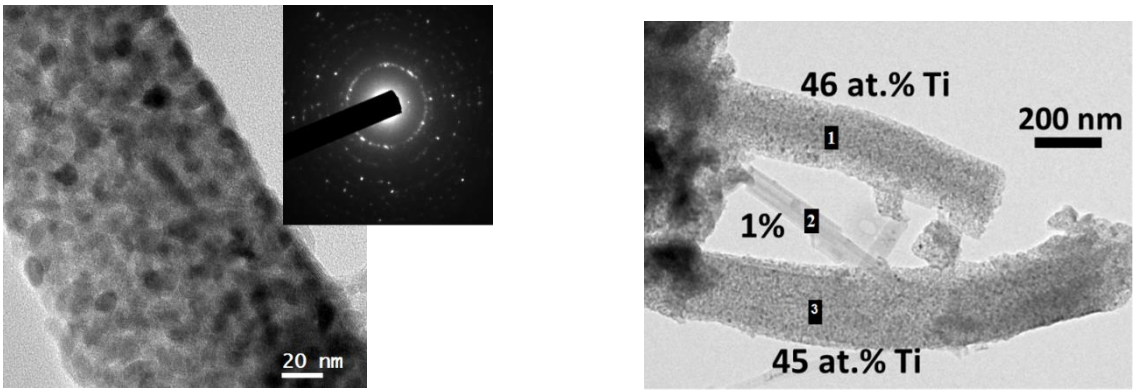

a) b)

Fig. 4: TEM micrographs and corresponding electron diffraction pattern indexed as TiO_2 anatase (a) and EDS local analysis showing uncoated (point 2) and uniformly coated point 1 and 3) palygorskite fibers (b).

3.3- Photocatalytic properties under UV light

The photocatalytic activity of different TiO_2–Pal composite samples elaborated by mechanosynthesis was tested towards the degradation under UV light of OG dye by using the laboratory set-up described in the experimental section (2.3). The results in Figure 5 showed that photocatalytic efficiency significantly increased with the amount of $TiOSO_4$ used in photocatalyst synthesis and thus the amount of TiO_2 present in TiO_2_Pal nanocomposite. This was evidenced by on one hand the strong decrease of OG concentration for instance in the first 10 min, revealing a high initial degradation rate of the pollutant around 2.6×10^{-2} s^{-1} for TiO_2/Pal mass ratio of 3.3/1 with respect to that determined for the mass ratio of 0.6/1 ($\approx1.5\times10^{-2}$ s^{-1}). On the other hand, the almost total elimination of the OG dye from the solution was achieved within about 2 h when using TiO_2/Pal mass ratio of 3.3/1 whilst almost 10% of the dye remained

after the same time of UV irradiation in presence of TiO_2/Pal mass ratio of 0.6/1 (but a plateau has not yet been reached).

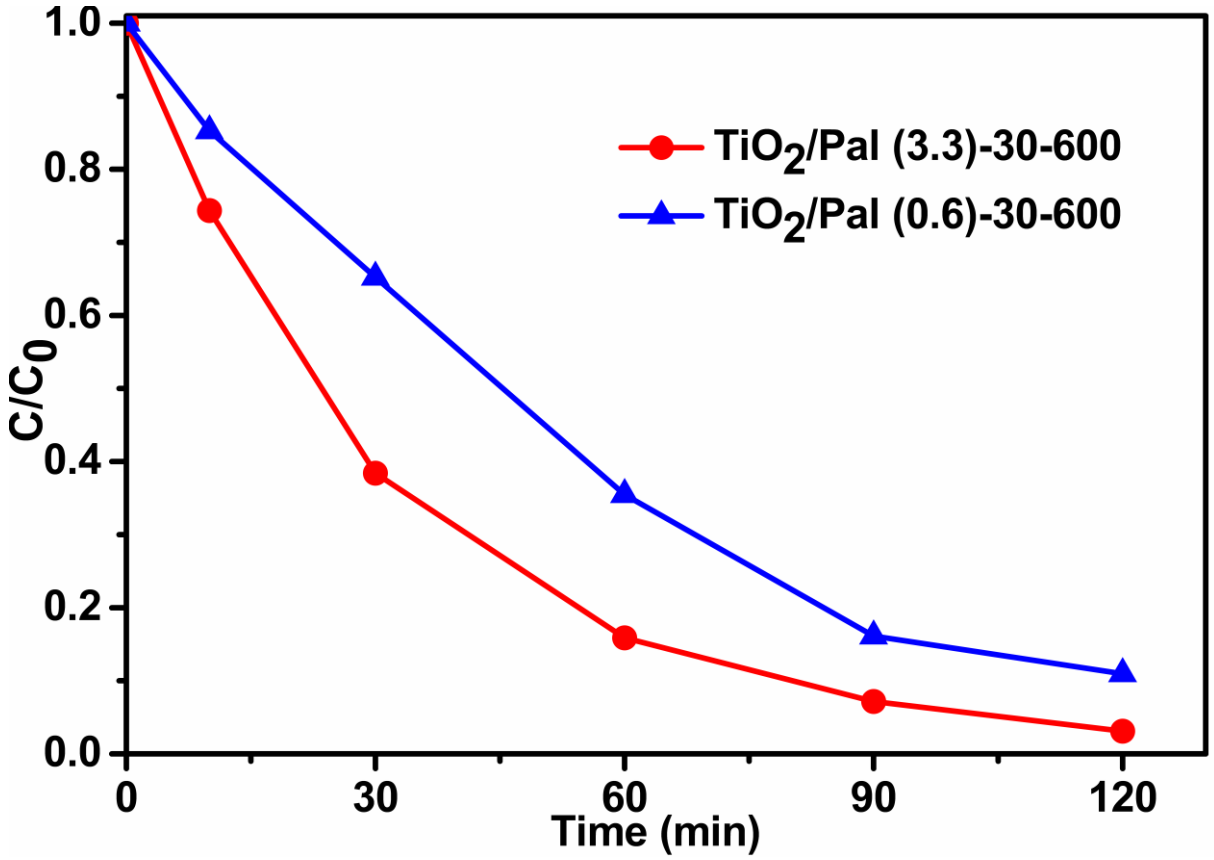

Fig. 5: Change in the concentration of OG (where C_0 and C denote the concentrations of OG at the initial time t = 0, and after an elapsed time t of the photocatalytic reaction) vs. UV irradiation time of the samples, differing in $TiOSO_4$/ Pal mass ratio (0.6/1 and 3.3/1), grinded during 30 min at 500 rpm and afterwards air annealed at 600°C for 1 h.

The influence of annealing temperature on the photocatalytic activity towards the removal of OG dye of TiO_2_Pal was afterwards studied on the most active one corresponding to TiO_2 /Pal mass ratio = 3.3/1. Figure 6 interestingly showed that the unheated as-milled Pal_$TiOSO_4$ mixture (sample Pal_TiO_2_(3.3)_30) already exhibited photoactivity under UV irradiation. Indeed, 50% of the initial quantity of OG decreased after 2 hours of irradiation. This is due to the formation of photoactive TiO_2 resulting, as beforehand mentioned, from the heterogeneous

solid-state reaction between $TiOSO_4$ and the carbonate phases (calcite + ankerite) present as accessory minerals in the Pal raw clay (reaction 1). Although the TiO_2 formed in as-grinded material was amorphous, as ascertained above by XRD, this is not exceptional since it was already shown that amorphous TiO_2 can be active in photocatalysis under UV irradiation [41]. Indeed, from a general point of view, even if amorphous semiconductors have less efficient electronic properties than their crystallized counterparts, they nevertheless find specific applications as in photovoltaic.

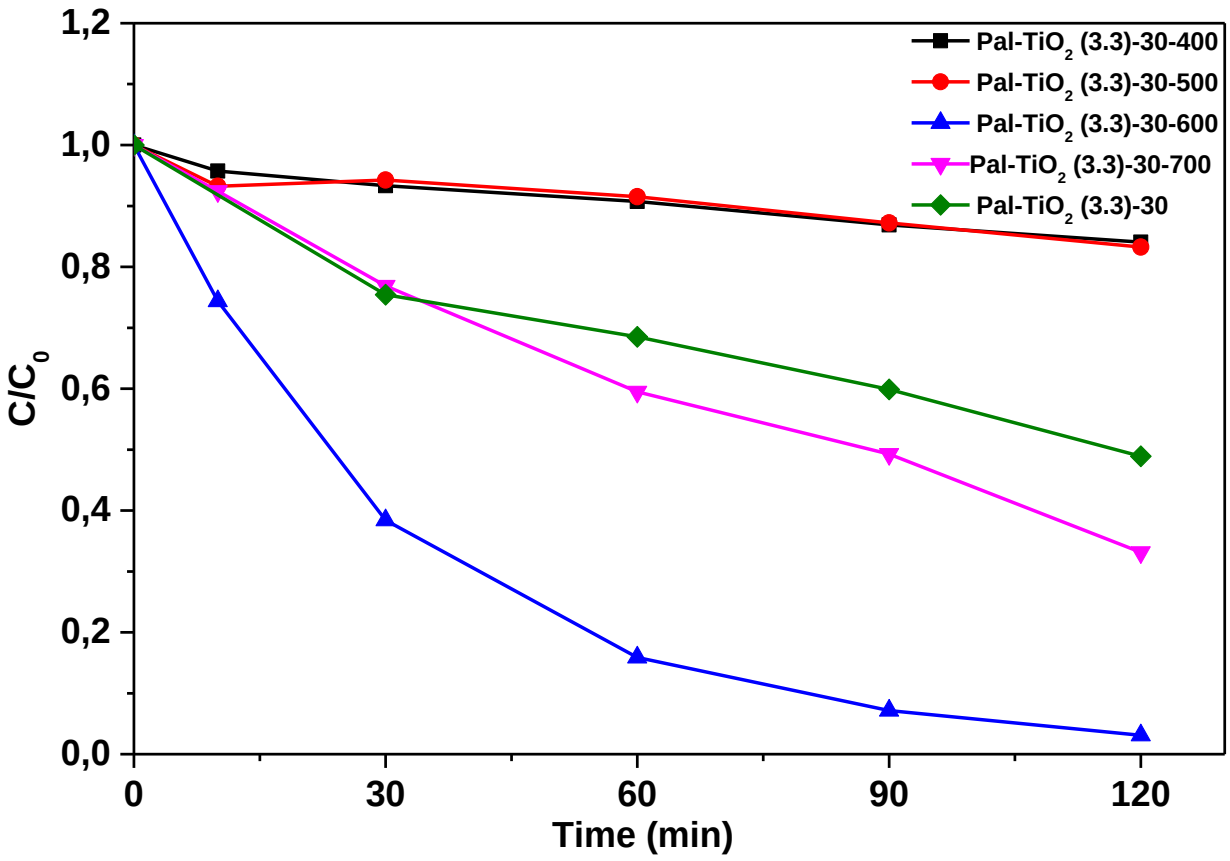

Fig. 6: Change in the concentration of OG vs. UV irradiation time of TiO_2_Pal elaborated by mechanosynthesis ($TiOSO_4$/Pal mass ratio = 3.3/1, grinding at 500 rpm for 30 min) and air annealing at 400, 500, 600 and 700°C.

Samples annealed at 400 and 500°C showed quite similar photo-degradation curves of the OG and paradoxically showed a lower photoactivity compared to as-grinded sample, allowing the removal of only 15% after 2 hours of illumination. This annealing temperature range is therefore insufficient to ensure a good crystallization of TiO_2 in the form of anatase but, on the other hand, it seems to be sufficient for inducing a detrimental diffusion of species that trap excitons (Pal clay cations for example), thus affecting the photocatalytic efficiency of the composite. Calcination at 600°C promoted the most efficient active palygorskite-supported TiO_2 photocatalyst since it allowed almost complete degradation of the OG after 2 hours of UV irradiation. This improvement was attributed to the good crystallinity of TiO_2 anatase upon the sample calcination at 600°C as confirmed above by XRD. On the other hand, when the sample was annealed at 700°C, photocatalytic activity again decreased. This reduction in photocatalytic activity may be due to the growth of TiO_2 particles beyond the optimal nanocrystalline size, which promotes the recombination of charge carriers. Also, a partial phase transformation of the more active anatase TiO_2 phase into the less photoactive rutile variety as reported by Bouna *et al.*, [29] and Rhouta *et al.*, [28] is not excluded although none of the corresponding peaks have yet been detected at 700°C, the presence of other crystalline phases can hide them.

3.4- Photocatalytic properties under sunlight

Owing to its high photoactivity under UV evidenced above by the tests on the laboratory set-up, the TiO_2_Pal nanocomposite with mass ratio TiO_2/Pal of 3.3/1 was thereafter retained for performing the study of photocatalytic activity under sunlight towards the removal of OG dye.

3.4.1- Activity under constant solar irradiation – indoor experiments

For studying optical properties of TiO_2-Pal, the change in transmittance (%), defined as the ratio of transmitted (I_t) to incident (I_i) intensities, was followed versus catalyst slurry mass concentration. Figure 7 showed that the necessary amount for the absorption of 90% of incident

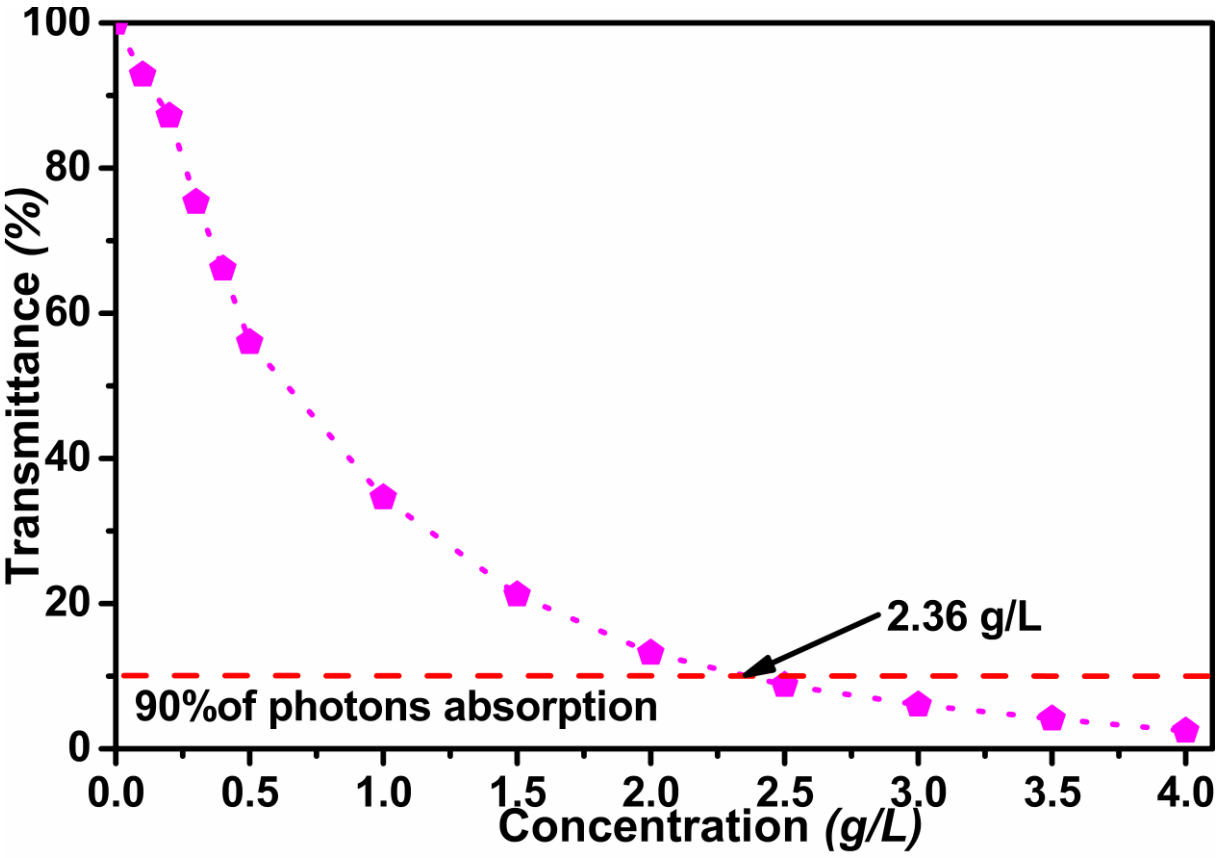

Fig. 7: Variation of transmittance in the spectral range 250 -1100 nm (artificial solar light 1000 $W.m^{-2}$) as a function of the catalyst dispersion concentration in an aqueous suspension.

light simulating sunlight (1000 W/m^2) for a catalyst dispersion thickness of 2 cm (C_{2cm}) was around 2.36 g/L, *i.e.* 1.34 g/L of TiO_2 taking into account its proportion of 57 wt% assessed by Individual Counting by single Particle (ICP) in the nanocomposite. Photocatalytic tests in batch mode using the indoor solar simulator described in the experimental section were performed by varying the amount of TiO_2_Pal dispersed in OG solution of 5 cm of thickness around the optimum amount ($C_{5cm} = 2/5 \times C_{2cm} \approx 0.95$ g/L) allowing maximum absorption.

Figure 8 showed that very low amount of TiO_2_Pal, *e.g.* 0.25 g/L, exhibited a relatively low photocatalytic activity leading to the removal of about only 40% of OG after 150 min of irradiation with an initial photo-degradation rate of about 5×10^{-3} s^{-1}. Nevertheless, by increasing the TiO_2_Pal mass concentration beyond 0.5 g/L up to 1.5 g/L, a better efficiency occurs and a quite similar photocatalytic behavior of the photocatalyst towards OG elimination was observed. Indeed, the OG photodegradation considerably increased as evidenced on one hand, by the strong decrease of OG concentration for instance in the first 20 min, revealing a high initial degradation rate ($\approx 7\times10^{-3}$ s^{-1}) of the pollutant and, on the other hand, by the elimination of almost 60% of OG dye from the solution within the same time of irradiation. These results showed that around the optimal mass concentration of TiO_2_Pal (≈ 0.95 g/L) beforehand determined by optical measurements, the catalyst exhibited maximal photoactivity for dye removal due to highest light absorption. Thus, an increase in the mass concentration of the photocatalysts beyond its optimal mass concentration is unnecessary since the maximum absorption of incident light has already been reached. This is in agreement with Plantard *et al.*, [42] who reported that for a given pollutant and a fixed initial concentration, the degradation kinetic constants obtained for the same photocatalyst depended solely on the quantity of photons absorbed. As a result, degradation by photocatalysis is function to the concentration of the catalyst in suspension, up to a threshold value at which all the incident radiation is almost absorbed.

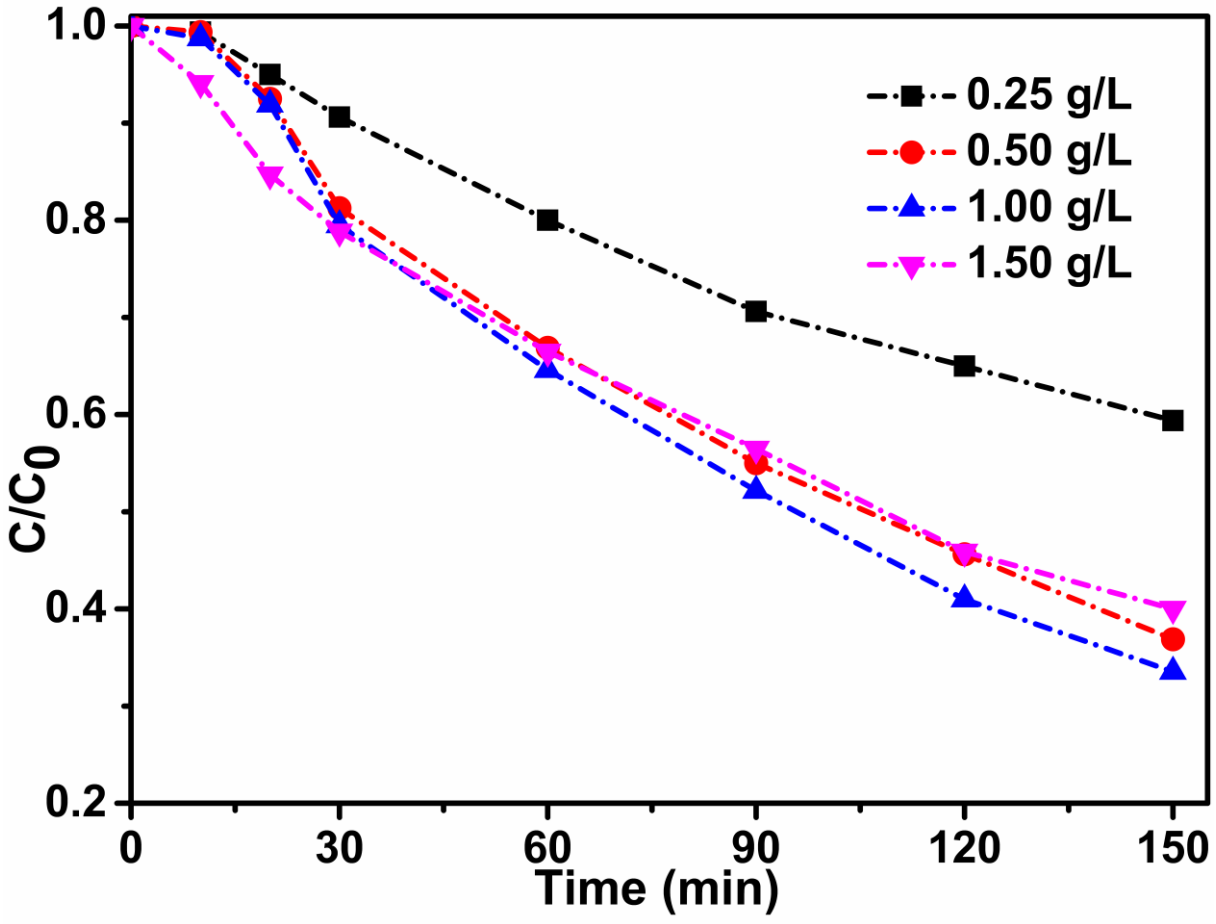

Fig. 8: Variation of the relative OG concentration versus time (where C_0 and C denote the OG concentrations at the initial time t = 0, and after an elapsed time t) in the 1000 $W.m^{-2}$ solar simulator recorded for different mass concentrations of the TiO_2_Pal composite photocatalyst.

Besides photocatalyst mass concentration in the aqueous suspension, photons fluxes also constituted a crucial parameter influencing heterogeneous photocatalysis process especially under solar light characterized by the variation of irradiation intensity. Figure 9, representing OG proportion change versus solar irradiation time at different photons fluxes in presence of 0.94 g/L of TiO_2_Pal revealed that in general, and as expected, an increase of the radiation intensity led to an increase of the OG pollutant degradation. This is the result of the increase of quantity of photons absorbed. It is obviously well known that this is only the UV part of the

448 solar spectrum that is effective for photocatalytic treatment with TiO_2 as active component.
449 With the solar simulator UV intensity is directly proportional to the total intensity delivered by
450 the lamp. It is almost the case for solar natural irradiation (even if the UV percentage is
451 influenced by the weather conditions). So, we made the choice to keep the total radiation
452 intensity received as the reference. It is the energy flux received by the surface of a reactor
453 working in outdoor conditions.
454
455 For being transposed to solar photocatalysis treatment, OG photodegradation kinetic should be
456 modulated taking into account the irradiation intensity key parameter. In photodegradation of a
457 target molecule (OG herein) using a slurry catalyst (TiO_2_Pal), rates can be approached by the
458 modified Langmuir-Hinshelwood (L-H) relationship (1) [43]:
459

460 $$\frac{\mathbf{dC}}{\mathbf{dt}} = \mathbf{k(I)}\frac{\mathbf{C}}{\mathbf{1+\beta.C}} = -(\boldsymbol{\alpha}.\frac{\mathbf{S}}{\mathbf{V_T}}.\mathbf{I})\frac{\mathbf{C}}{\mathbf{1+\beta.C}} \qquad (1)$$

461 With k(I) the apparent kinetic constant (s^{-1}) function of the intensity, C the OG concentration
462 ($g.L^{-1}$), β ($L.g^{-1}$) a constant determined by comparison between calculated and experimental
463 data. In the simplest case, k(I) is directly proportional to the intensity I received by unit volume
464 of solution (V_T in L) with an irradiated surface S (m^2). α ($J.L^{-1}$) is the second unknown
465 parameter. If necessary, a dependence of k according to a law in power of the irradiation can
466 be introduced to account of additional limiting phenomena such as the charge recombination.

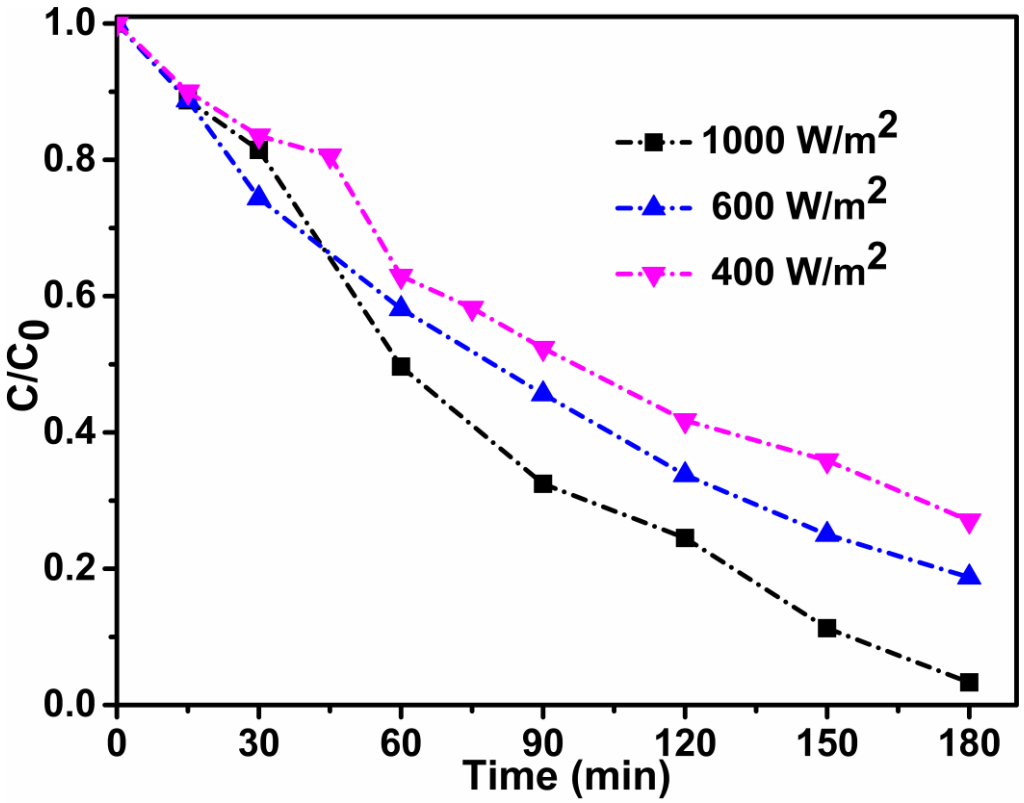

Fig. 9: Variation of the OG proportion versus time (s) upon irradiation simulating sunlight at 400, 600 and 1000 W.m^{-2} in presence of TiO_2_Pal (0.94 g/L) composite photocatalyst.

For a constant irradiation intensity, the integration of equation (1) leads to the expression (2):

$$f\left(\frac{C}{C_0}, \beta\right) = \ln\left(\frac{C}{C_0}\right) + \beta . C_0 . \left(\frac{C}{C_0} - 1\right) = -k(I) . t \qquad (2)$$

To be valuable, the value of β has to be constant whatever is the irradiation. It is determined simply by considering the left part of equation 2 depends linearly on time. Figure 10 depicted experimental profiles of the logarithmic adimensional concentration C/C_0 as a function of the time with a value of β = 0.65 L.g^{-1}. It showed linear dependence with a satisfactory agreement. This ascertained pseudo first-order kinetics whose the slope k depends on the intensity of the irradiation according to the relationship (3).

$$k(I) = \frac{S}{V_T} . \alpha . I \qquad (3)$$

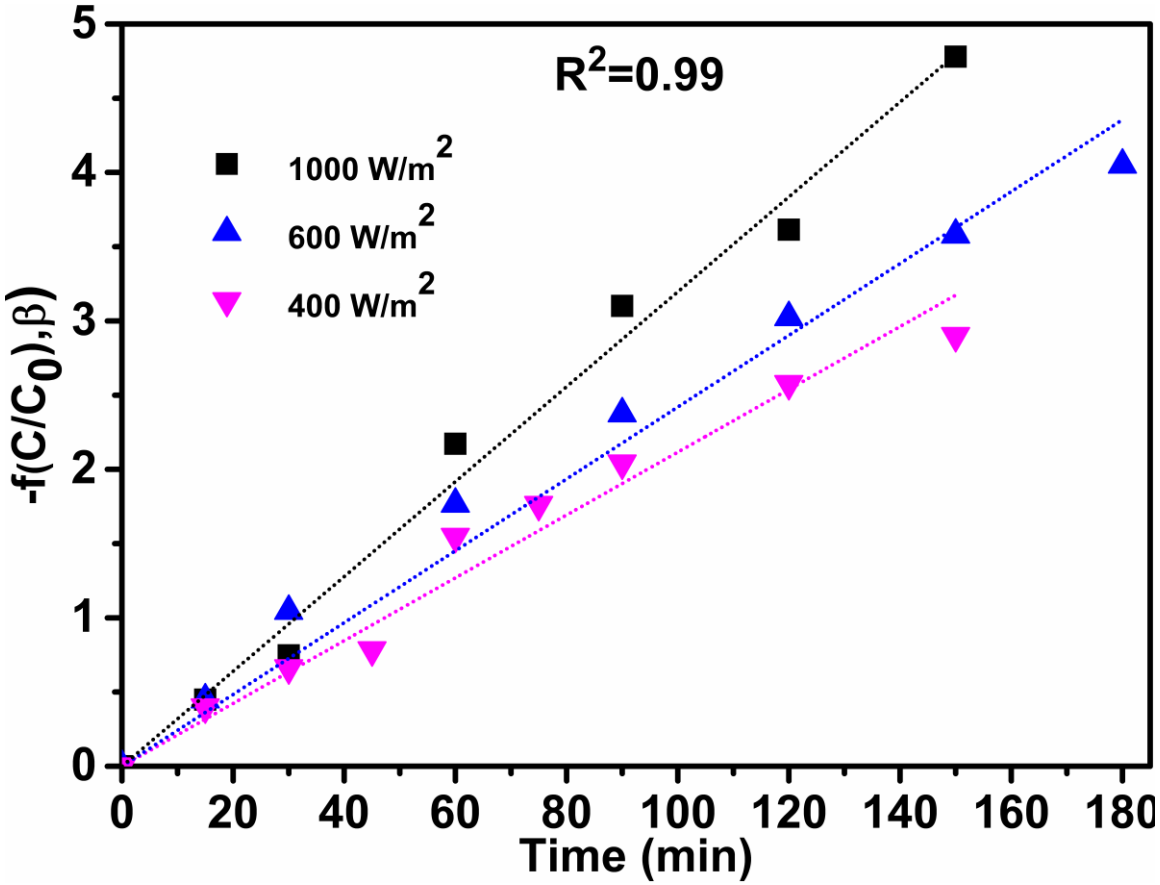

Fig.10: Linear variation of $Ln(C/C_0)$ of OG versus time (s) for different irradiation intensities simulating sunlight in the presence of 0.94 g/L of TiO_2_Pal catalyst for β = 0.65 $L.g^{-1}$ confirming a pseudo first order kinetics. Continuous colored lines represent the best agreement between the experimental data and a linear regression for each level of irradiation.

Likewise, the variation of the apparent kinetic constant k versus irradiation intensity (I) (Fig. 11) showed a linear trend supported by a reasonable degree of accuracy of about 0.99. Hence, the value of the kinetic constant (α), deduced from the slope, can be assessed to be around 1.5 L/kJ.

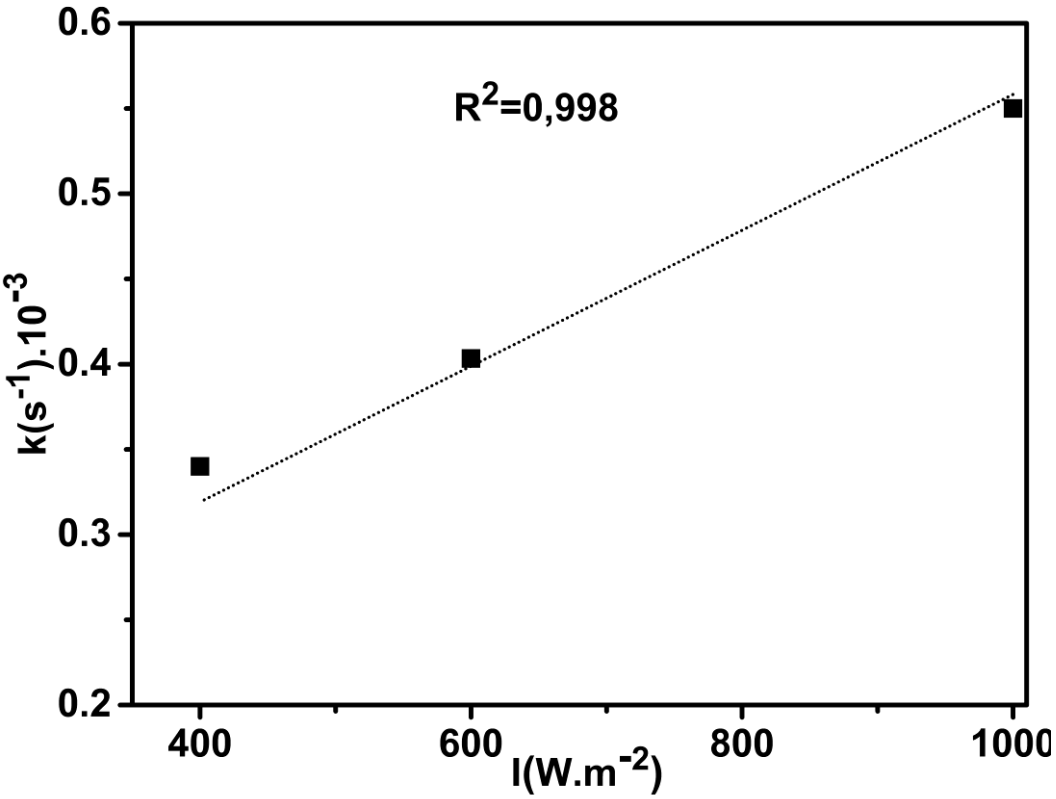

Fig. 11: Linear variation of the kinetic constant k of OG photodegradation versus the irradiation intensity I simulating sunlight onto TiO_2_Pal photocatalyst slurry. The continuous gray line simulates the data according to equation (3).

By introducing the values of α and β in the expression (2), the C/C_0 plots versus time show a very good fitting between the experimental and simulated data for all irradiation flux densities, as expected from the good agreement already reported in Figures 10 and 11. This result validates the proposed kinetic model described by equation (2).

3.4.2- Activity under natural discontinuous irradiation - outdoor solar pilot

The photocatalytic tests for the removal of OG dye from aqueous solution were carried out in presence of TiO_2_Pal slurry by using an outdoor solar pilot and according to conditions described in the experimental section (2.3). Nonetheless, owing to the variation of solar

irradiation along a day, the change of OG dye during these tests should be versus the cumulative energy Q_g ($J.L^{-1}$) received by the reactor given by the relationship (4) [44]:

$$Q_g = \frac{S}{V_T} \cdot \int_0^{t_i} I(t)\, dt \qquad (4)$$

with t_i (s) the time at which an aliquot was taken for being centrifuged and analyzed by the spectrophotometer and I(t) the solar irradiation intensity measured over time using the sensors mounted on the pilot as described in the experimental section.

Figure 12 shows, like data obtained with the indoor solar simulator in "batch" mode, a decrease in OG dye proportion upon solar irradiation, which thus confirms the photoactivity of TiO_2_Pal under solar light. In this respect, 50% of the OG dye was removed with a cumulated energy of 74.2 kJ/L whilst the total removal of the dye required a cumulated energy of 250 kJ/L.

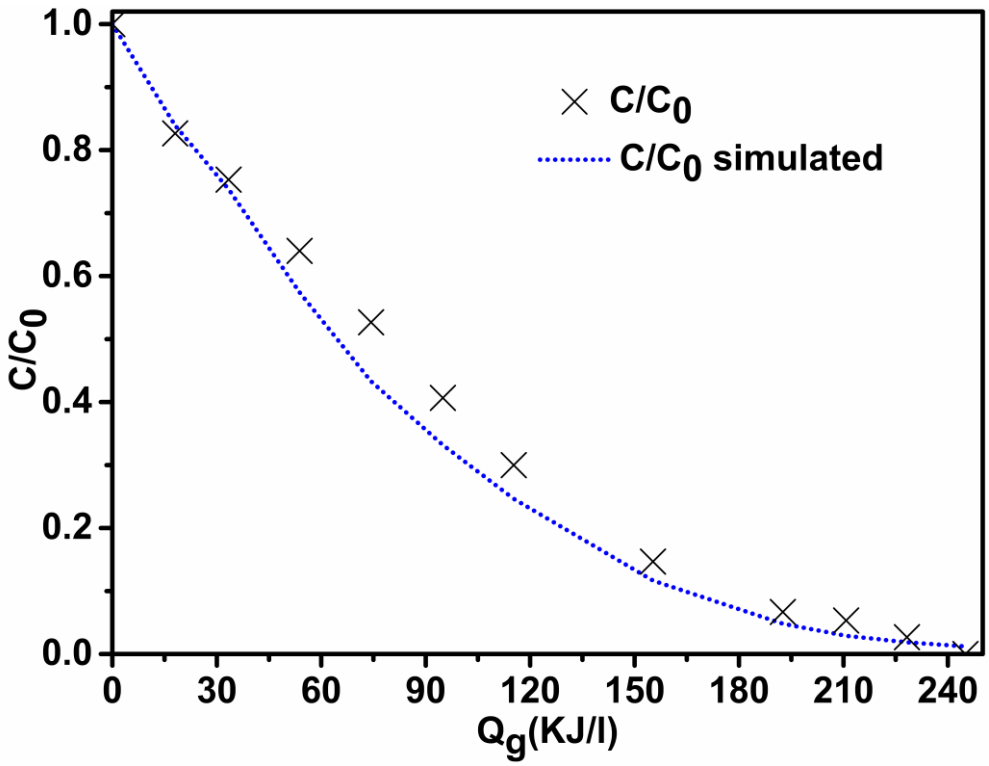

Fig. 12: Change of the experimental relative concentration of the OG (×) and simulated data (dotted curve) versus the total cumulated energy obtained for TiO_2_Pal composite photocatalyst.

Besides, by introducing the numerical values of α (1.5 L/kJ) and β (0.65 $L.g^{-1}$) beforehand determined in the relationship (5) derived from the above one (2) after substituting I(t) by $Q_g(t)$, a good agreement between simulated and experimental data was observed with a good degree of accuracy.

$$\frac{C(t)}{C_0} = e^{-[(\alpha \ \frac{S}{V_T} Q_g(t)) + (\beta C_0 (\frac{C}{C_0} - 1)]} \quad (5)$$

This confirmed the validation of the kinetic model proposed and ascertained that the OG photodegradation in presence of TiO_2_Pal slurry was of first order with a kinetic constant of **1.5** L/kJ and did not involve adsorption phenomenon.

4. Conclusion

TiO_2 photocatalyst supported onto natural palygorskite clay mineral fibers (TiO_2_Pal) was successfully elaborated by a one-pot dry mechanical method. This elaboration process is very interesting because it directly uses palygorskite clay without the multiple purification steps that wet processes frequently required. Furthermore, it is solvent free, eco-friendly and based on smart *in situ* solid-state reaction between carbonates accessory minerals contained in the raw clay and a cheap molecular Ti precursor. As a result, it can be easily scaled up to an economically viable large-scale production.

Structural analysis and microstructural characterization using XRD and TEM respectively showed that TiO_2_Pal, revealed homogeneous monodisperse TiO_2 NPs in the form of anatase wrapping palygorskite fibers. This sample was shown to be the most photoactive under UV irradiation towards the removal of OG dye from aqueous solution upon the use of a laboratory set-up. Then photocatalytic tests carried out by an indoor solar simulator set-up on OG dye solution containing an optimal mass concentration of TiO_2_Pal nanocomposite was found to

assure the maximum of the elimination of OG. In this respect, a good agreement was demonstrated between experimental and simulated data using a pseudo first order kinetic model for the dye photodegradation. The same photocatalytic behavior was also obtained with an outdoor solar pilot confirming the photoactivity of these supported TiO_2_Pal photocatalysts under sunlight.

Acknowledgements:

The financial supports from the "Programme d'Action Intégrée Volubilis" (N° 14/SM/14) and the Project of PPR-CNRST “Domaines Prioritaires de la Recherche Scientifique et du Développement Technologique" (PPR1/2015/63) are gratefully acknowledged.

References

[1] P.K.J. Robertson, Semiconductor photocatalysis: an environmentally acceptable alternative production technique and effluent treatment process, J. Clean. Prod. 4 (1996) 203–212. doi:10.1016/S0959-6526(96)00044-3.

[2] J. Herrmann, Heterogeneous photocatalysis: fundamentals and applications to the removal of various types of aqueous pollutants, Catal. Today. 53 (1999) 115–129. doi:10.1016/S0920-5861(99)00107-8.

[3] A. Fujishima, T.N. Rao, D.A. Tryk, Titanium dioxide photocatalysis, 1 (2000) 1–21. doi:10.1016/S1389-5567(00)00002-2.

[4] A. Fujishima, X. Zhang, Titanium dioxide photocatalysis: present situation and future approaches, Comptes Rendus Chim. 9 (2006) 750–760. doi:10.1016/j.crci.2005.02.055.

[5] Y. Paz, Preferential photodegradation - why and how?, Comptes Rendus Chim. 9 (2006) 774–787. doi:10.1016/j.crci.2005.03.032.

[6] O. Carp, Photoinduced reactivity of titanium dioxide, Prog. Solid State Chem. 32 (2004) 33–177. doi:10.1016/j.progsolidstchem.2004.08.001.

[7] R. Ghosh Chaudhuri, S. Paria, Visible light induced photocatalytic activity of sulfur doped hollow TiO_2 nanoparticles, synthesized via a novel route, Dalt. Trans. 43 (2014) 5526–5534. doi:10.1039/c3dt53311e.

[8] M.A. Alvarez Lemus, H. Monroy, T. López, E.N. De la Cruz Hernández, R. López-González, Effect of surface modification on the bioactivity of sol–gel TiO_2-based nanomaterials, J. Chem. Technol. Biotechnol. 91 (2016) 2148–2155. doi:10.1002/jctb.4915.

[9] C.B.D. Marien, C. Marchal, A. Koch, D. Robert, P. Drogui, Sol-gel synthesis of TiO_2 nanoparticles: effect of Pluronic P123 on particle's morphology and photocatalytic degradation of paraquat, Environ. Sci. Pollut. Res. 24 (2017) 12582–12588.

doi:10.1007/s11356-016-7681-2.

[10] A. Moiseev, M. Krichevskaya, F. Qi, A.P. Weber, J. Deubener, Analysis of photocatalytic performance of nanostructured pyrogenic titanium dioxide powders in view of their polydispersity and phase transition: Critical anatase particle size as a factor for suppression of charge recombination, Chem. Eng. J. 228 (2013) 614–621. doi:10.1016/j.cej.2013.05.038.

[11] A.H. Mamaghani, F. Haghighat, C.S. Lee, Hydrothermal/solvothermal synthesis and treatment of TiO2 for photocatalytic degradation of air pollutants: Preparation, characterization, properties, and performance, Chemosphere. 219 (2019) 804–825. doi:10.1016/j.chemosphere.2018.12.029.

[12] T. Umebayashi, T. Yamaki, H. Itoh, K. Asai, Band gap narrowing of titanium dioxide by sulfur doping, Appl. Phys. Lett. 81 (2002) 454. doi:10.1063/1.1493647.

[13] T. Umebayashi, T. Yamaki, S. Yamamoto, A. Miyashita, S. Tanaka, T. Sumita, K. Asai, Sulfur-doping of rutile-titanium dioxide by ion implantation: Photocurrent spectroscopy and first-principles band calculation studies, J. Appl. Phys. 93 (2003) 5156–5160. doi:10.1063/1.1565693.

[14] P. Billik, G. Plesch, V. Brezová, L. L'Kuchta, M. Valko, M. Mazúr, Anatase TiO2 nanocrystals prepared by mechanochemical synthesis and their photochemical activity studied by EPR spectroscopy, J. Phys. Chem. Solids. 68 (2007) 1112–1116. doi:10.1016/j.jpcs.2007.02.010.

[15] P. Billik, G. Plesch, Mechanochemical synthesis of anatase and rutile nanopowders from TiOSO4, Mater. Lett. 61 (2007) 1183–1186. doi:10.1016/j.matlet.2006.06.080.

[16] M. Čaplovičová, P. Billik, Ľ. Čaplovič, V. Brezová, T. Turáni, G. Plesch, P. Fejdi, On the true morphology of highly photoactive anatase TiO2 nanocrystals, Appl. Catal. B Environ. 117–118 (2012) 224–235. doi:10.1016/j.apcatb.2012.01.010.

[17] M. Houari, M. Saidi, D. Tabet, P. Pichat, H. Khalaf, The Removal of 4-chlorophenol and Dichloroacetic Acid in Water Using Ti-, Zr- and Ti/Zr-Pillared Bentonites as Photocatalyst, Am. J. Appl. Sci. 2 (2005) 1136–1140. doi:10.3844/ajassp.2005.1136.1140.

[18] J. Liu, M. Dong, S. Zuo, Y. Yu, Solvothermal preparation of TiO_2/montmorillonite and photocatalytic activity, Appl. Clay Sci. 43 (2009) 156–159. doi:10.1016/j.clay.2008.07.016.

[19] M. Nieto-Suárez, G. Palmisano, M.L. Ferrer, M.C. Gutiérrez, S. Yurdakal, V. Augugliaro, M. Pagliaro, F. del Monte, Self-assembled titania–silica–sepiolite based nanocomposites for water decontamination, J. Mater. Chem. 19 (2009) 2070. doi:10.1039/b813864h.

[20] T. An, J. Chen, G. Li, X. Ding, G. Sheng, J. Fu, B. Mai, K.E. O'Shea, Characterization and the photocatalytic activity of TiO2 immobilized hydrophobic montmorillonite photocatalysts, Catal. Today. 139 (2008) 69–76. doi:10.1016/j.cattod.2008.08.024.

[21] P. Aranda, R. Kun, M.A. Martín-Luengo, S. Letaïef, I. Dékány, E. Ruiz-Hitzky, Titania−Sepiolite Nanocomposites Prepared by a Surfactant Templating Colloidal Route, Chem. Mater. 20 (2008) 84–91. doi:10.1021/cm702251f.

[22] B. Rhouta, H. Kaddami, J. Elbarqy, M. Amjoud, L. Daoudi, F. Maury, F. Senocq, A. Maazouz, J.-F. Gerard, Elucidating the crystal-chemistry of Jbel Rhassoul stevensite (Morocco) by advanced analytical techniques, Clay Miner. 43 (2008) 393–403. doi:10.1180/claymin.2008.043.3.05.

[23] L. Bouna, B. Rhouta, M. Amjoud, A. Jada, F. Maury, L. Daoudi, F. Senocq, Correlation between eletrokinetic mobility and ionic dyes adsorption of Moroccan stevensite, Appl. Clay Sci. 48 (2010) 527–530. doi:10.1016/j.clay.2010.02.004.

[24] O. Lakbita, B. Rhouta, F. Maury, F. Senocq, M. Amjoud, A. Jada, L. Daoudi, ,

644 Supported Photocatalyst Based on CuO – TiO_2/Palygorskite Nanocomposite Material
645 for Wastewater Treatment, J. Colloid Sci. Biotechnol. 5 (2016) 1–7.
646 doi:10.1166/jcsb.2016.1150.
647 [25] O. Lakbita, B. Rhouta, F. Maury, F. Senocq, M. Amjoud, L. Daoudi, On the key role of
648 the surface of palygorskite nanofibers in the stabilization of hexagonal metastable β-
649 Ag_2CO_3 phase in palygorskite-based nanocomposites, Appl. Clay Sci. 172 (2019).
650 doi:10.1016/j.clay.2019.02.023.
651 [26] W. Xie, G. Zhang, B. Mu, Z. Tanga, J. Zhang, The promoting effect of palygorskite on
652 CeO_2-WO_3-TiO_2 catalyst for the selective catalytic reduction of NOx with NH_3, Appl.
653 Clay Sci. 192 (2020) 1–10. doi:10.1016/j.clay.2020.105641.
654 [27] A. Wu, D. Wang, C. Wei, X. Zhang, Z. Liu, P. Feng, X. Ou, Y. Qiang, H. Garcia, J.
655 Niu, A comparative photocatalytic study of TiO_2 loaded on three natural clays with
656 different morphologies, Appl. Clay Sci. 183 (2019) 1–12.
657 doi:10.1016/j.clay.2019.105352.
658 [28] B. Rhouta, L. Bouna, F. Maury, F. Senocq, M.C. Lafont, A. Jada, M. Amjoud, L.
659 Daoudi, Surfactant-modifications of Na^+-beidellite for the preparation of TiO2-Bd
660 supported photocatalysts: II-Physico-chemical characterization and photocatalytic
661 properties, Appl. Clay Sci. 115 (2015) 266–274. doi:10.1016/j.clay.2015.04.025.
662 [29] L. Bouna, B. Rhouta, M. Amjoud, F. Maury, M.-C. Lafont, a. Jada, F. Senocq, L.
663 Daoudi, Synthesis, characterization and photocatalytic activity of TiO_2 supported
664 natural palygorskite microfibers, Appl. Clay Sci. 52 (2011) 301–311.
665 doi:10.1016/j.clay.2011.03.009.
666 [30] B. Rhouta, E. Zatile, L. Bouna, O. Lakbita, F. Maury, L. Daoudi, M.C. Lafont, M.
667 Amjoud, F. Senocq, A. Jada, A. Aït Aghzzaf, Comprehensive physicochemical study
668 of dioctahedral palygorskite-rich clay from Marrakech High Atlas (Morocco), Phys.

669 Chem. Miner. 40 (2013) 411–424. doi:10.1007/s00269-013-0579-3.
670 [31] L. Bouna, B. Rhouta, L. Daoudi, F. Maury, M. Amjoud, F. Senocq, M.C. Lafont, a.
671 Jada, a. A. Aghzzaf, Mineralogical and Physico-Chemical Characterizations of
672 Ferruginous Beidellite-Rich Clay from Agadir Basin (Morocco), Clays Clay Miner. 60
673 (2012) 278–290. doi:10.1346/CCMN.2012.0600305.
674 [32] L. Bouna, B. Rhouta, F. Maury, A. Jada, F. Senocq, M.-C. Lafont, Photocatalytic
675 activity of TiO_2/stevensite nanocomposites for the removal of Orange G from aqueous
676 solutions, Clay Miner. 49 (2014) 417–428. doi:10.1180/claymin.2014.049.3.05.
677 [33] K. Hofstadler, R. Bauer, S. Novalic, G. Heisler, New Reactor Design for Photocatalytic
678 Wastewater Treatment with TiO_2 Immobilized on Fused-Silica Glass Fibers:
679 Photomineralization of 4-Chlorophenol, Environ. Sci. Technol. 28 (1994) 670–674.
680 doi:10.1021/es00053a021.
681 [34] C. Sarantopoulos, E. Puzenat, C. Guillard, J.-M. Herrmann, A.N. Gleizes, F. Maury,
682 Microfibrous TiO_2 supported photocatalysts prepared by metal-organic chemical vapor
683 infiltration for indoor air and waste water purification, Appl. Catal. B Environ. 91
684 (2009) 225–233. doi:10.1016/j.apcatb.2009.05.029.
685 [35] O. Lakbita, B. Rhouta, F. Maury, F. Senocq, M. Amjoud, L. Daoudi, Influence of the
686 crystal structure of Ag_2CO_3 on the photocatalytic activity under visible light of
687 Ag_2CO_3-Palygorskite nanocomposite material, Appl. Surf. Sci. 464 (2019) 205–211.
688 doi:10.1016/j.apsusc.2018.09.053.
689 [36] L. Bouna, B. Rhouta, F. Maury, Physicochemical Study of Photocatalytic Activity of
690 TiO_2 Supported Palygorskite Clay Mineral, 2013 (2013) 2–7.
691 doi.org/10.1155/2013/815473
692 [37] F. Correia, V. Goetz, G. Plantard, D. Sacco, A model for solar photocatalytic
693 mineralization, J. Sol. Energy Eng. Trans. ASME. 133 (2011) 2–6.

694 doi:10.1115/1.4004242.
695 [38] G. Plantard, T. Janin, V. Goetz, S. Brosillon, Solar photocatalysis treatment of
696 phytosanitary refuses: Efficiency of industrial photocatalysts, Appl. Catal. B Environ.
697 115–116 (2012) 38–44. doi:10.1016/j.apcatb.2011.11.034.
698 [39] G. Plantard, V. Goetz, Correlations between optical, specific surface and photocatalytic
699 properties of media integrated in a photo-reactor, Chem. Eng. J. 252 (2014) 194–201.
700 doi:10.1016/j.cej.2014.04.055.
701 [40] T. Janin, V. Goetz, S. Brosillon, G. Plantard, Solar photocatalytic mineralization of 2,4-
702 dichlorophenol and mixtures of pesticides: Kinetic model of mineralization, Sol.
703 Energy. 87 (2013) 127–135. doi:10.1016/j.solener.2012.10.017.
704 [41] Z.-G. Sun, X.-S. Li, X. Zhu, X.-Q. Deng, D.-L. Chang, A.-M. Zhu, Facile and Fast
705 Deposition of Amorphous TiO_2 Film under Atmospheric Pressure and at Room
706 Temperature, and its High Photocatalytic Activity under UV-C Light, Chem. Vap.
707 Depos. 20 (2014) 8–13. doi:10.1002/cvde.201307088.
708 [42] G. Plantard, V. Goetz, D. Sacco, TiO_2-coated foams as a medium for solar catalysis,
709 Mater. Res. Bull. 46 (2011) 231–234. doi:10.1016/j.materresbull.2010.11.011.
710 [43] J.M. Herrmann, Photocatalysis fundamentals revisited to avoid several misconceptions,
711 Appl. Catal. B Environ. 99 (2010) 461–468. doi:10.1016/j.apcatb.2010.05.012.
712 [44] S. Malato, J. Blanco, A. Vidal, C. Richter, Photocatalysis with solar energy at a pilot-
713 plant scale: An overview, Appl. Catal. B Environ. 37 (2002) 1–15. doi:10.1016/S0926-
714 3373(01)00315-0.
715 [45] P. Aranda, R. Kun, M.A. Martín-Luengo, S. Letaïef, I. Dékány, E. Ruiz-Hitzky,
716 Titania−Sepiolite Nanocomposites Prepared by a Surfactant Templating Colloidal
717 Route, Chem. Mater. 20 (2008) 84–91. doi:10.1021/cm702251f.
718 [46] B. Rhouta, L. Bouna, F. Maury, F. Senocq, M.C. Lafont, A. Jada, M. Amjoud, L.

719 Daoudi, Surfactant-modifications of Na^{+}–beidellite for the preparation of TiO_2–Bd
720 supported photocatalysts: II—Physico-chemical characterization and photocatalytic
721 properties, Appl. Clay Sci. 115 (2015) 266–274.
722 doi:http://dx.doi.org/10.1016/j.clay.2015.04.025.
723